PERGAMON

Chaos, Solitons and Fractals 14 (2002) 917–928

CHAOS
SOLITONS & FRACTALS

www.elsevier.com/locate/chaos

Applications of fractal geometry and renormalization group to the Italian seismic activity

Alberto Carpinteri *, Bernardino Chiaia, Stefano Invernizzi

Department of Structural Engineering and Geotechnics, Politecnico di Torino, Corso Duca Degli Abruzzi 24, 10129 Torino, Italy

Accepted 13 March 2002

Communicated by Prof. Amr Elnashai FREng

Abstract

In the past two decades, Fractal Geometry developed as a new and powerful mathematical tool able to model a wide class of complex natural systems. Particularly, when joined with renormalization techniques, Fractal Geometry represents the natural and synthetic way to characterize the so-called self-organized processes, emphasizing their universality and the scaling laws arising at the critical points. Nevertheless, the choice of the most relevant seismic parameter is often not trivial, as in the case of Italian seismicity, where magnitude must be replaced by the seismic energy release, in order to obtain unambiguous multifractal spectra. Moreover, to model the stick-slip phenomenon, it is useful to consider the contact mechanics of self-affine rough faults. A numerical model provides the exact distribution of normal and tangential forces at any rough surface. The Renormalization Group technique represents the theoretical framework able to explain the multifractal distribution of contact micro-forces obtained numerically. As a consequence, the experimentally detected multifractal release of seismic energy derives directly from the mechanical work of a multifractal distribution of forces during the slip event.

1. Introduction

Large geodynamical processes are currently explained by means of the Theory of Plate Tectonics, which was developed a few decades ago. Within that conceptual framework, it is possible to give a unitary foundation to various phenomena like earthquakes, the derive of continents, and orogenic processes, otherwise described by independent, and often disagreeing, models. According to the hypothesis of Plate Tectonics, crustal deformations take place at the boundary between the major surfacial plates, where the highest concentration of faults, volcanoes and earthquakes is experienced. In this introduction, some experimental evidences of fractality in the field of seismology are briefly described. Furthermore, the most important phenomenological models from the literature are outlined.

1.1. Fractals in seismology

The fractal character of self-organized critical phenomena like earthquakes is often revealed by power-law constitutive equations relating the physical quantities involved in the process [8]. For example, the precursor signals of the largest earthquakes are described by power-laws, which means that there is not a characteristic time scale, because all (temporal) scales are relevant to the cooperative process. From a mathematical point of view, it can be observed that

* Corresponding author. Tel.: +39-11-5644828; fax: +39-11-5644899.
E-mail address: carpinteri@polito.it (A. Carpinteri).

0960-0779/02/$ - see front matter
PII: S0960-0779(02)00081-4

any parameter $\varepsilon(t)$, describing seismic activity, recorded at a certain time t close to that of the catastrophic event t_c, can be expressed by the following power law:

$$\varepsilon(t) = A + B(t_c - t)^{\gamma}, \tag{1}$$

where γ is the so-called *critical exponent*. For example, this behaviour has been recognized when considering temporal sequences of fore-shocks, as a function of their magnitude.

One of the most used statistical relations describing the frequency occurrence of earthquakes, as a function of their magnitude, is the well-known logarithmic [14] equation

$$\log \dot{N} = -bm + \log \dot{a}, \tag{2}$$

where $\dot{a}$ and b are empirical constants, and $\dot{N}$ is the temporal frequency of earthquakes with magnitude greater than m, within a certain geographical area. While the constant b depends on the characteristics of the seismo-genetic zone, the constant $\dot{a}$ can be assumed as an index of the local seismicity. Eq. (2) can be integrated with respect to the time and written in terms of N and a (i.e., by considering a finite period). Moreover, the Gutenberg–Richter equation well applies to different geographical extensions, scaling up to entire regions. For instance, the frequency of earthquakes in the Italian territory [7] is shown, as a function of the magnitude, in Fig. 1(a). It is worth noting that only above a threshold magnitude (in this case equal to 5) the experimental data are adequately fitted by Eq. (2).

The magnitude m, although representing the most common quantity adopted, does not always provide a deep understanding of the problem. Thus, other parameters can be introduced, with more relevant physical meaning [29]. For example, the *seismic moment* M, which can be obtained as a function of the magnitude m by means of the following empirical equation:

$$\log M = cm + d, \tag{3}$$

where c and d are non-dimensional constants, respectively equal to 1.5 and 9.1. On the other hand, the seismic moment can be expressed as a function of the *rupture area* A , through the following power-law:

$$M = \beta A^{3/2}, \tag{4}$$

where β is another non-dimensional constant [17]. Eqs. (2)–(4) can be merged together to emphasize that the relation between the frequency of the earthquakes with magnitude greater than m and the corresponding rupture area, is still a power-law with fractional exponent

$$\dot{N} = \dot{\gamma} A^{-3b/2c}. \tag{5}$$

The above relation can be compared with the classical *scaling* of an Euclidean smooth area ($A \sim d^2$), and therefore it is possible to determine the *fractal dimension* D of the domain on which the seismic phenomenon takes place [29]:

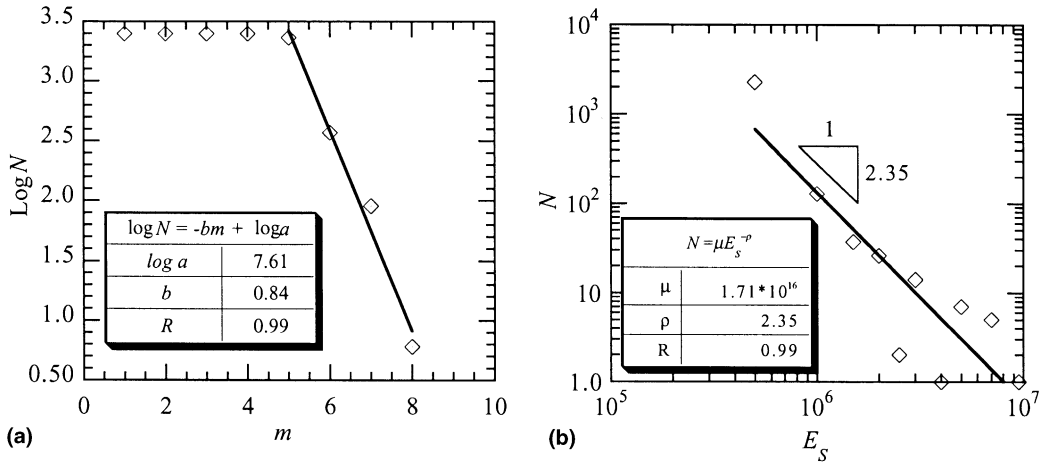

Fig. 1. Logarithmic diagram of the absolute frequency N of earthquakes vs. their magnitude m in the Italian territory (a); bi-logarithmic diagram of the frequency N vs. the released energy E_S (b).

$$D = \frac{3b}{c} \cong 2b. \tag{6}$$

Since, in most cases, $c = 1.5$, the fractal dimension is simply equal to the value $2b$.

A power-law is encountered also when the seismic energy E_S, released during the earthquake in the form of seismic waves, is considered [29]. In fact, in analogy with the seismic moment (Eq. (3)), the energy can be written as a logarithmic function of the magnitude

$$\log E_S = 1.44m + 5.24, \tag{7}$$

where E_S is measured in Joule. Fig. 1(b) shows that the frequency of the earthquakes occurred in the Italian area, with energy equal or greater than E_S, can be well fitted by a power-law. Furthermore, the fractal dimension of the seismic process is equal to one half of the slope in the bi-logarithmic diagram, i.e., $D \cong 1.66$.

The fractal dimension of the seismic process depends directly on the fractal dimension of the fault network where the phenomenon takes place. The fractal dimension of a fault network can be calculated experimentally, as reported in [23]. Typically, the fractal dimension of the seismic process is strictly lower than the fractal dimension of the fault network. Some authors tried to explain this difference based on the hypothesis that only a subset of the fault web is *active* from the seismic point of view [26].

In addition, the spatial distribution of epicentres shows a marked complexity. Although experimental results are not always univocal, some authors emphasized the *multifractal* distribution of earthquake magnitude within a homogeneous area [11]. As will be explained in the next sections, the magnitude m is not the best seismic parameter to consider with regards to the spatial distribution of the process. On the contrary, the released seismic energy E_s seems to be much more effective to this purpose, similarly to the study of the rupture area distribution (see Eq. (7)).

The temporal correlation between the *after-shocks* recorded after a big earthquake, has a fractal character. The mean frequency of *after-shocks* $\dot{N}$ is inversely proportional to the time t elapsed after the main shock

$$\dot{N}(t) = (t + c)^{-\xi}, \tag{8}$$

where c is a non-dimensional constant and the exponent ξ is usually fractional. Eq. (8) is known as the Omori's Law [22].

Further evidences of fractality in the seismic process can be found when experimental seimograms are considered. The experimental wide band spectra cannot be explained by simple models like those based on the hypothesis of smooth fault nucleation. As will be shown in Section 4, the complex geometry of the contact surface must be considered [18,32], together with the cooperative aspects of the sliding phenomenon.

From the experimental point of view, it is worth to mention the wide literature on the statistics of earthquake precursors (*fore-shocks*) [12,30]. In this case, there is no agreement among the scientists regarding the usefulness of any efforts devoted to earthquake forecasting, as confirmed by the recent *Nature's* debate [19].

1.2. Fundamental mechanical models of earthquakes

The first mechanical model of fault behaviour, able to explain at least the principal features of the seismic process, was the homogeneous and continuous *Reid Model*, also known as the *Elastic Rebound Theory* [24]. According to this theory, elastic deformation accumulates in the neighbourhood of the faults, due to the relative shear displacement of the adjacent plates. When the shear strength of the fault is reached, the strain energy is suddenly released, triggering the earthquake. Although the continuum model is able to catch some important features of the process, it fails in describing the so-called *stick-slip* behaviour, where the relative displacements on the fault plane are discontinuous and failure can be triggered by a cascade of small local ruptures and displacements.

Later, in 1967, the famous *Spring-Masses Model* [6] was put forward, to describe the cooperative aspects of the phenomenon. The mechanical interactions occurring on the fault plane were represented by a discrete set of rigid masses linked together by elastic springs. Moreover, the motion was transmitted to the masses by a rigid body with a very slow constant velocity (simulating the global motion of tectonic plates), and contact was described by the classical Coulomb's law. The dynamics of such a system is not uniform at all. Movements of any extent take place suddenly (*stick-slip* behaviour), and wide displacements are triggered by a cascade process starting from small localized events. The same complex patterns can be obtained by considering one single block, provided that the potential energy of the system is a non-smooth fractal function like, for example, the *devil's staircase function* [20].

More recently, within the framework of the *Theory of Complexity*, the seismic phenomenon has been recognized as a *self-organized* critical process. Therefore, contrarily to other critical processes (i.e., phase transitions), the critical state does not require the fine tuning of some global state variable (like the temperature), for its activation. Instabilities take

place as soon as a local threshold is reached, and a cooperative phenomenon develops, spreading over all scales. Due to the lack of a characteristic length scale, critical events are well described by the typical power-law frequency distribution. The archetype of the so-called *self-organized criticality* (SOC) is the *sand-pile model* [1]. This model shows astonishing similarity with the seismic process, such that, recently, some Researchers [21] simulated not only the temporal statistics (such as the Gutenber–Richter or the Omori laws), but also the spatio-temporal correlation of seismic events.

Interesting results have been obtained also in the framework of the *Renormalization Group Theory* [27]. This theory developed in the field of quantum mechanics and was subsequently applied to various problems, such as phase transitions, fluid dynamics and statistical physics. It is based on scale-invariance and can be considered as the physical counterpart of fractal geometry. In particular, the concept of *discrete scale invariance* or *log-periodicity* is based on the assumption that the exponent of the power-law, describing any global variable close to the critical point, is a non-integer complex number. Therefore, the classical power-law is replaced by the following modulated function

$$\varepsilon - K = A(t_c - t)^d \left[1 + C\cos\left(\left(2\pi \frac{\log(t_c - t)}{\log p} \right) + \Psi \right) \right], \tag{9}$$

where ε is the *Benioff strain release*, Ψ, C and K are experimental constants, p and d are the scaling exponents, and t_c the estimated time of occurrence of the catastrophic event. This approach seems to substantially improve the reliability of earthquake predictions [2].

2. The multifractal formalism

The notion of *multifractal measures* developed during the last two decades. A complete and detailed description of the formalism can be found in the specific literature [10]. This section outlines only the aspects of the procedure that were implemented in our numerical computations. In a few words, a multifractal set is represented by the non-homogeneous distribution of a certain quantity over a (fractal) support, characterized by a peculiar scaling behaviour represented by the "*spectrum*" of the dimensions.

2.1. The spectrum of fractal dimensions D_q

Some authors [13] have proposed a generalization of the different definitions of fractal dimension by introducing the *generalized fractal dimension* D_q. Its generic expression, as a function of the parameter q, is the following:

$$D_q = \frac{\tau(q)}{1-q}, \tag{10}$$

where $\tau(q)$ is the *sequence of the mass exponents*. The graph of D_q (shown in Fig. 2(a)) is constant and equal to the topological dimension when Euclidean sets are considered. Also for classical mono-fractal sets, D_q is constant and equal to the fractal dimension. Finally, for multifractal sets, D_q is a monotonic decreasing function, respectively equal to the

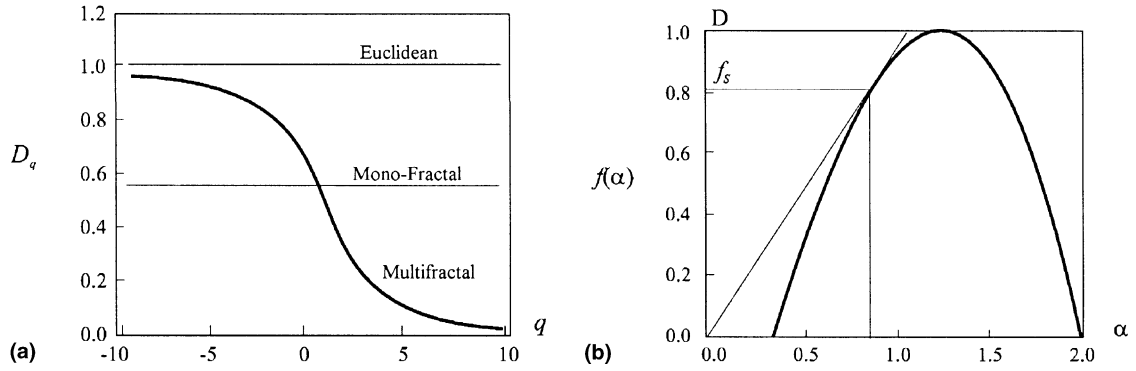

Fig. 2. Generalized fractal dimension (a); Multifractal spectrum of a one-dimensional multiplicative process (b).

fractal dimension of the support for $q = 0$, to the information entropy for $q = 1$, and to the *correlation dimension* for $q = 2$.

2.2. The sequence of mass exponents $\tau(q)$

In order to develop a consistent numerical algorithm for the determination of the multifractal spectra of experimental data, it is useful to introduce the *generalized box-counting method*. In this case, each covering box is weighted by its measure content, and raised to the exponent q. Consider a generic set S, composed of N points, as an estimate of the distribution to be analysed. If $\mu_i = N_i/N$ is the *probability* of the ith box to be counted, then the *sequence of the mass exponents* is the following:

$$\tau(q) = -\lim_{\delta \to 0} \frac{\log\left(\sum_i \mu_i^q\right)}{\log(\delta)}. \tag{11}$$

Thereby, it is straightforward to obtain the generalized fractal dimension, except when $q = 1$ and Eq. (10) becomes singular. In that case, the following expression must be used:

$$D_{q=1} = \lim_{\delta \to 0} \frac{\sum_i \mu_i \log(\mu_i)}{\log(\delta)}. \tag{12}$$

2.3. The Lipshitz–Hölder exponent α

One way to characterize the singularity of a certain measure $M(x)$ distributed over a multifractal set is the so-called *Lipshitz–Hölder exponent* α. The multifractal measure is, in general, a singular non-decreasing function that is differentiable if $\alpha = 1$, constant if $\alpha > 1$, whereas it is singular if $0 \leqslant \alpha < 1$. Moreover, it is possible to represent any multifractal set S as the direct summation of the subsets S_α, containing the points with the same singularity exponent α, which have fractal dimension equal to $f(\xi(\alpha))$. The graph of $f(\alpha)$ is the so-called *multifractal spectrum*, as shown in Fig. 3(b). It is characterized by some peculiar properties. The maximum of the multifractal spectrum is, in general, equal to the dimension of the support . Furthermore, the point of the graph with derivative equal to 1 refers to the particular subset where the measure concentrates. The dimension $f(\alpha_S)$ of this subset is known as the *information dimension* or *entropy* of the distribution. It is possible to show that the measure of this subset is practically equal to the whole

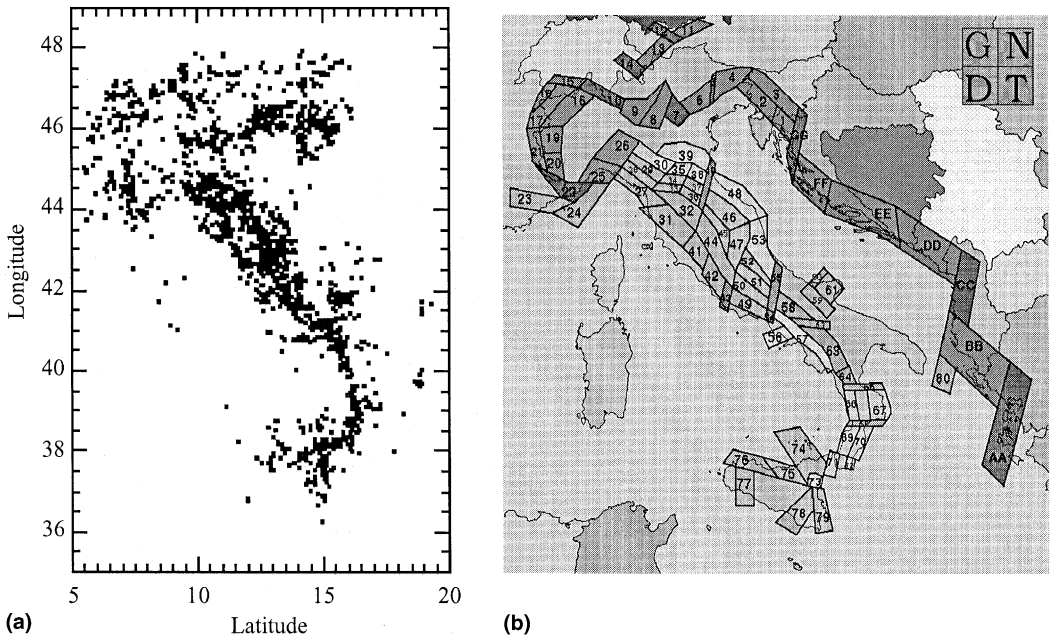

Fig. 3. Distribution of the epicentres of earthquakes in the Italian area (a); Homogeneous seismo-genetic zones (b).

measure, because of the extreme rarefaction of the subsets with a great, or very poor, measure content μ_i. Finally, the *multifractal spectrum* $f(\alpha)$ can be easily obtained as the *Legendre transform* of the *sequence of the mass exponents*.

3. An application: the multifractal analysis of the Italian catalogue of earthquakes

The Italian catalogue of destructive earthquakes (NT4.1 and its following integrations) has been developed in the past decade by the Italian Group for the Defence against Earthquakes (GNDT) [7], with the aim of progressively substituting the previous historical descriptive catalogues. In order to avoid the ambiguity that has been found by other authors, the released seismic energy E_s will be considered in our analysis instead of the magnitude m. In fact, despite of its historical relevance, the magnitude does not represent directly the energetic content burst by the earthquake. Following the same arguments used to emphasize the fractal character of the Gutenberg–Richter relation (see Eq. (7)), the seismic energy appears to be the best parameter if the multifractality of the seismic process has to be put into evidence.

Another originality of our analysis is represented by the numerical algorithm previously described, which allows the direct calculation of the spectrum of the generalized fractal dimensions, as well as of the multifractal spectrum, without the need of calculating correlation integrals, which are necessary in other approaches [13].

The first analysis concerned the entire catalogue. The position of epicentres is assigned by the relative latitude and longitude (Fig. 3), whereas the seismic energy is calculated from the magnitude by applying Eq. (7). In order to perform the numerical computation, the seismic energies have been previously normalized. The graph of the generalized fractal dimension is shown in Fig. 4(a). The monotonic decreasing trend, characteristic of multifractal sets, is clearly recognized, as well as the asymptotic behaviour for very high or very low values of the exponent q. The fractal dimension of the support over which the seismic processes take place can be obtained for $q = 0$, and is equal to $D_0 = 1.36$. Moreover, the information dimension is equal to $D_1 = 1.28$. It is worth noting that almost all of the seismic energy is released on such fractal subset. Finally, the correlation dimension is equal to $D_2 = 1.19$. The multifractal spectrum, obtained by means of the *Legendre transform*, is shown in Fig. 4(b). The typical downward concavity of the spectrum confirms the multifractality of the analysed set. Furthermore, it is possible to obtain the fractal dimension of each subset as a function of the measure singularity.

Recently, Eneva [9] has noticed that spurious multifractal spectra can sometimes emerge from mono-fractal distributions (i.e., different seismo-genetic zones) as the result of an additive process. In order to take also this aspect into account, the multifractal analysis has been performed also on single homogeneous seismo-genetic zones (see Fig. 5). Although the results appear more scattered because of the limited data sets, the same qualitative patterns have been obtained. Therefore, in the case of the Italian catalogue, the observed multifractality cannot be ascribed to spurious additive effects.

4. Mechanical modelling of self-affine fault

The mechanical models previously described show that the local slip law assumed for the single fault plays a leading role both in the temporal forecasting of catastrophic seismic events and in the evaluation of the seismic energy release.

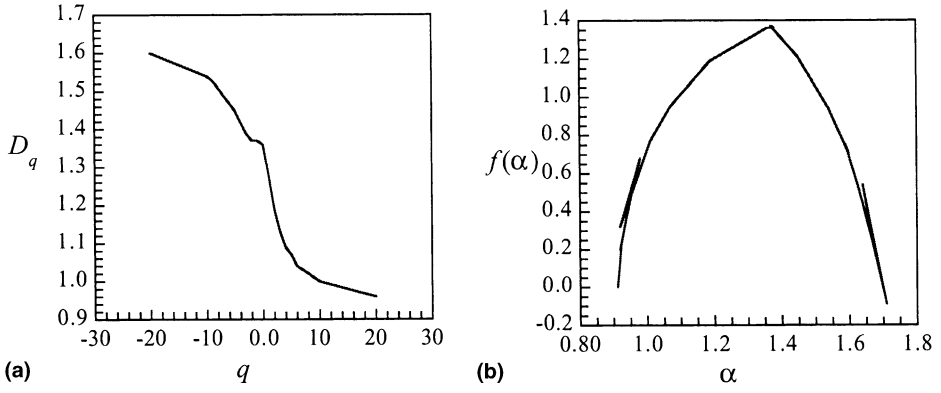

Fig. 4. Analysis of the Italian earthquake catalogue: generalized fractal dimensions of the seismic energy release (a); multifractal spectrum (b).

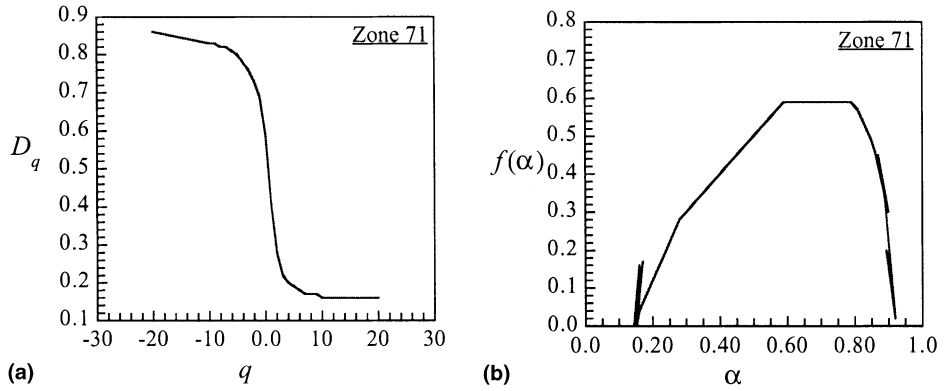

Fig. 5. Analysis of the seismo-genetic zone 71: generalized fractal dimensions of the seismic energy release (a); multifractal spectrum (b).

Unfortunately, a simple slip law is not sufficient to encompass the statistical dispersion of the asperity strength all over the fault plane, neither to simulate the complexity of earthquake statistics [25]. In fact, the *self-affinity* of the contact surface morphology within a fault must be considered, as well as the *self-organization* of the slip phenomenon, where slip events occur at all scales interacting with each other and eventually leading to a catastrophic collapse.

Some recent results in the modelization of the contact mechanics of rough surfaces seem to be particularly promising [4,5]. In fact, the authors were able to simulate the mechanical interaction of two elastic half-spaces in contact through *self-affine* fractal interfaces (Fig. 6(a)). The contact domains (Fig. 6(b)), obtained numerically, result to be *lacunar fractals* (i.e., their fractal dimension is less than 2), and their *self-similar* fractal topology is responsible for the well-known size effect on the shear strength of natural interfaces (like those involved in rock slopes, shear instabilities and fault sliding).

In this section, attention is focussed on the normal contact between elastic half-spaces with self-affine interfaces, while in the next section also tangential micro-forces will be considered. The multifractal analysis shows that the distribution of the normal micro-forces within a lacunar contact domain is a multifractal set. In particular, by increasing the global normal force, the maximum of the multifractal spectrum increases (Fig. 7(a)). In fact, the fractal dimension of the support (i.e., of the contact domain) increases and tends to the topological dimension (i.e., to $D = 2$) when an infinite force is applied (saturation of the contact domain). In addition, the shape of the multifractal spectrum becomes wider due to new asperities that progressively come into contact while the oldest contact asperities increase their micro-forces. On the other hand, by increasing the relative tangential shift of the opposing surfaces (under constant normal force), the density of the contact domain rapidly decreases (Fig. 7(b)). Therefore, the maxima of the spectra decrease and the spectra become narrower.

In the spirit of the renormalization group approach, the obtained result can be extended to the scale of tectonic faults. It is reasonable to assume that the energy release is proportional to the local contact force. Thereby, this simple

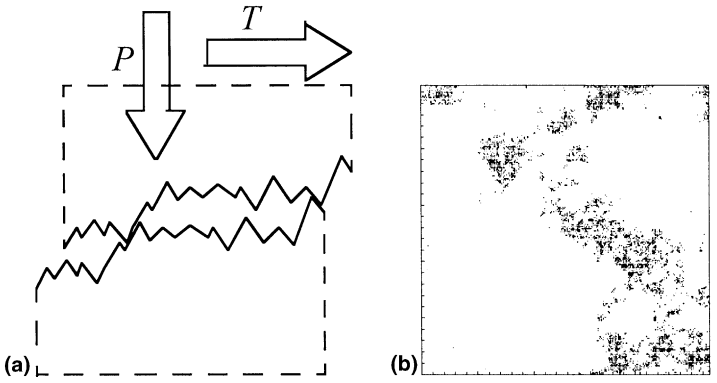

Fig. 6. Scheme of the normal and tangential interaction of self-affine faults (a); lacunar contact domain obtained numerically (b).

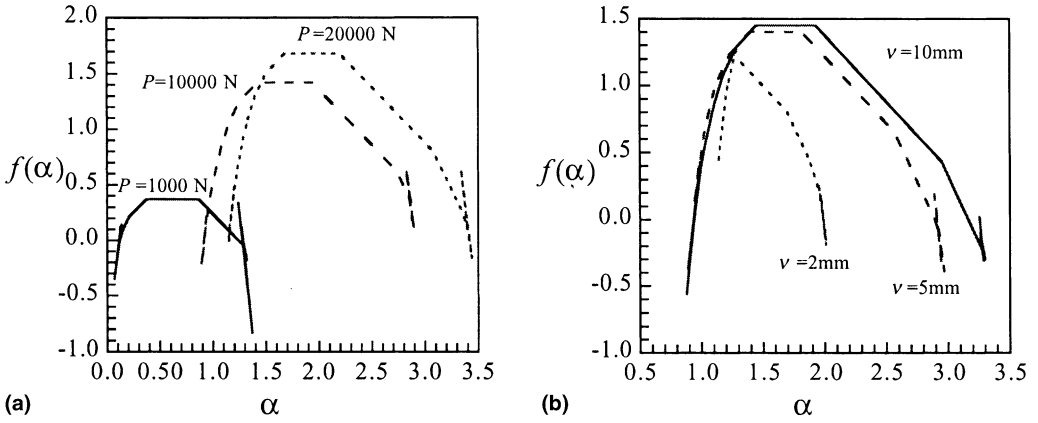

Fig. 7. Multifractal spectra of the contact micro-forces: increasing the normal force P with fixed relative position (a); constant normal force with varying horizontal shift v (b).

contact model is able to explain, at least, some of the multifractal patterns previously obtained by analysing historical seismic data.

5. Fault sliding as a critical phenomenon

The tangential force–displacement process can be treated as a critical phenomenon, by exploiting the properties of *self-similarity* of the contact domain. This kind of criticality already appears in other approaches [16,31], where, however, the peculiar multiscale mechanisms were not considered.

A simple renormalization group calculation provides interesting results regarding the onset of full-sliding and the scaling of the tangential force. The present approach is based on the one developed by Smalley et al. [28] to model the stick-slip behaviour of faults due to asperity failure, although there are two major differences. First, we deal with a (lacunar) fractal domain of contact points (resulting from the mechanical interaction of elastic self-affine half-spaces shown in Fig. 6), instead of an Euclidean array of asperities. Moreover, if Coulomb friction is supposed to hold at the micro-scales, we do not need to make assumptions on the shear strength distribution, since we exactly know, at any point, the value of the normal force and thus of the limit shear stress. On the other hand, a statistical distribution of shear strengths can also be introduced if the hypothesis of adhesive contact is made.

The fractal hierarchical model is built up according to the scheme reported in Fig. 8(b), and can be obtained by overlapping the subsequent box-coverings depicted in Fig. 8(a). The first-order cell (microscale) corresponds to the finest resolution, and subsequent orders are obtained by dyadic sequence. At the rth scale of observation, a generic

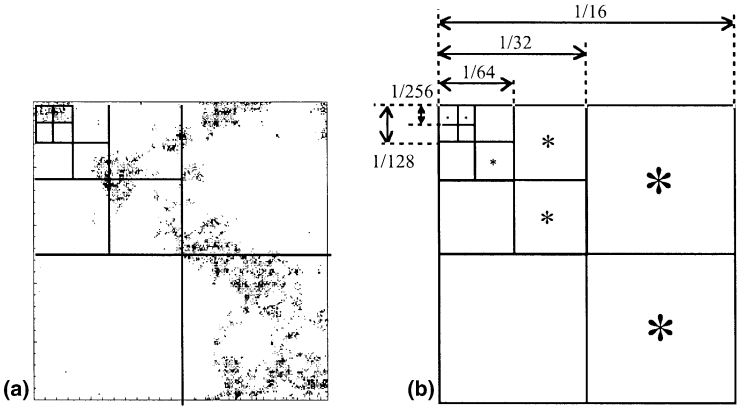

Fig. 8. Covering of the lacunar contact domain (a); and scheme of the renormalization procedure (b).

contact point corresponds to several contact points at the lower scale $(r-1)$th. Note that some cells are blank (i.e., there is no asperity) due to the lacunarity of the contact domain. There self-similarity is not an assumption, as in the case of [28], but is inherent to the model.

The starting point of the calculation is represented by computing the tangential stresses τ at any point of the contact domain, for a given value of the external tangential force T, by means of a discretized version of the Mindlin–Cattaneo method [3]. The tangential solution is obtained only at the smallest scale because, due to scale invariance, solutions at larger scales are naturally obtained from the renormalization process. Once the point with the highest $\tau/\tau_{\lim}$ ratio is determined, the external load is re-scaled to make this point reach exactly its critical condition. Therefore, the stresses at all the contact points are re-scaled in the spirit of linear elasticity. Once the first point has slipped, a certain amount of the stress it was carrying needs to be redistributed. From the physical point of view, stress transfer within the fault may be ascribed to the elastic energy release due to micro-slip, to the drop of the friction coefficient, or to any partial (or even complete) loss of load carrying capacity.

It is worth noting that, without stress transfer, the behaviour of the system is trivial and coincides with the Cattaneo's theory. We assume for simplicity that, at any scale, stress redistribution can occur only among the points within a box (the points which represent, at the larger scale, a single contact area). However, due to the renormalization procedure, non-local correlations are not restricted to the size of a cell but can spread to larger scales by exploiting self-similarity. Thus, the assumption of finite-size interactions is not restrictive and makes the problem mathematically treatable.

As in the case of fibrous materials [15], where it was shown that a composite material fails catastrophically after only a few strands have failed, also in the case of natural faults full-slip occurs much before all the points have reached their critical condition, due to stress redistribution. *Therefore, contrarily to the classical Cattaneo–Mindlin's theory, the limit shear value of a fault is smaller than the sum of the local shear strengths of the asperities* or, which is the same, the apparent global friction coefficient ($f_{\text{glob}} = T/P$) is smaller than the microscopic one f.

The renormalization procedure has been applied to several contact domains, characterized by different values of the fractal dimension Δ_S. For each contact domain, two different models of micro-friction have been adopted, namely Coulomb's friction and simple adhesion.

5.1. Microscopic Coulomb's friction

If Coulomb's friction is supposed to hold at the micro-scale, each asperity in contact can slip only when the shear stress reaches its critical value $\tau_{\lim}$, proportional to the normal contact stress $p(\tau_{\lim} = fp)$. Therefore, the distribution of strengths coincides with the distribution of normal micro-forces, which is multifractal (as shown in the previous section).

In our approach, we assume that, once a point has slipped, the friction coefficient f drops to a value $f' = \beta f$, where $\beta < 1$ is the redistribution coefficient (Fig. 9(a)). Thus, an amount of stress equal to $(1-\beta)fp$ has to be redistributed among the contact points in the cell. As a first approximation, we assume that this quantity is equally carried by the rest of the contact points in the cell. If another asperity, in the same cell, reaches its critical condition, this slips too, and some extra shear stress must be transferred. According to the renormalization procedure, we assume that an rth order cell slips only if all the corresponding points at the $(r-1)$th level have slipped. This circumstance depends on the

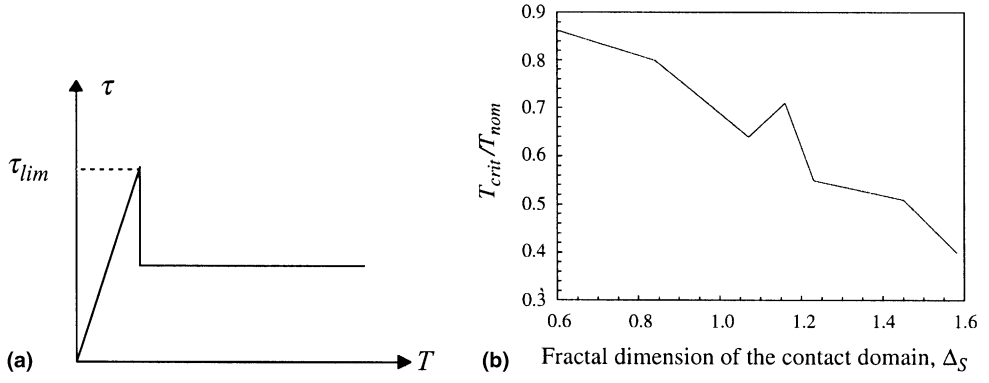

Fig. 9. Schematic drop of the friction coefficient after sliding of an asperity (a); decrease of the ratio $T_{\text{crit}}/T_{\text{nom}}$ as the fractal dimension of the contact domain increases (in the case of Coulomb's friction) (b).

applied shear stress, but also on the spatial distribution of the contact points and, differently from the adhesive hypothesis, also on the distribution of the normal micro-forces. The same calculations are repeated at subsequently larger scales, the collective behaviour at a certain level representing the input for the larger one.

Two situations can be obtained, that is, the micro-slip events can be confined below a certain scale (partial-slip), or they can spread virtually to any scale (full-sliding). The separating value of the shear force is the critical shear T_{crit}. From the practical point of view, this value can be numerically approximated, to the desired precision, by means of upper and lower bounds. It is interesting to compare the value of the critical shear T_{crit} with the value of the nominal shear strength T_{nom} predicted by Cattaneo's theory (no redistribution), which is equal to the sum of the local shear strengths, i.e., to $T_{\text{nom}} = fP$. For the domain depicted in Fig. 8(a) ($\Delta_S = 1.21$), in the case of $\beta = 0.8$ we have obtained $T_{\text{crit}} = 0.89T_{\text{nom}}$. In the case of ($\beta = 0.7$, T_{crit} is equal to $0.76T_{\text{nom}}$, and for $\beta = 0.6$, T_{crit} is only $0.49T_{\text{nom}}$. Thus, as one could easily expect, the higher the stress redistribution, the smaller the critical load. Clearly, below T_{crit}, the shapes of the stick and slip areas become remarkably different from the ones predicted by Cattaneo's theory.

5.2. Microscopic adhesion

The theory of adhesion states that friction, although independent of the apparent macroscopic area, is proportional to the true contact area and thus results primarily from adhesive bonding at true contact points. The bonding force is supposed to be independent of the normal force acting on each contact point.

We assume that, if the shear micro-force attains the bonding strength on a certain asperity, this point slips and carries no more shear. Thus, its stress has to be totally redistributed among the other contact points in the cell. Again, we assume that this stress must be equally carried only by the remaining contact points in the cell. If another asperity, in the same cell, reaches its critical condition, it slips too, and some extra shear stress must be transferred. As in the previous case, we assume that an rth order cell slips only if all the corresponding points at the $(r-1)$th level have slipped. The same calculations are repeated at the larger scales, by iteration to infinite order.

Two situations can be obtained also in this case, namely the micro-slip events can be confined below a certain scale (*partial-slip*), or they can spread virtually to any scale (*full-sliding*). The separating value of the shear force, which can be numerically approximated to the desired precision, is again the critical shear force T_{crit}.

If the adhesion strength is supposed to be constant within the fault, a rather brittle behaviour is obtained, namely full-slip is reached as soon as only a few points have slipped. This situation is, however, still less brittle than the fracture occurring in homogeneous materials, because the marked lacunarity of the contact domain provides a certain amount of ductility. More realistically, a statistic distribution of bonding strengths can be considered. We chose a classical quadratic Weibull distribution, stating that the probability P_a that the bonding strength τ_{lim} at a certain point is less than $a\tau$ is given by

$$P_a = 1 - \mathrm{e}^{-(ax)^2}, \tag{13}$$

where $x = \tau/\tau_0$ and τ_0 is a reference shear stress. In this case, the nominal shear strength T_{nom} is equal to the sum of the local shear strengths, i.e., to $T_{\text{nom}} = \sum(\tau_{\text{lim}}) = N\tau_{\text{mean}}$, where N is the number of contact points, and τ_{mean} is the mean value of the bonding strength. Following the analytical calculations by Smalley et al. [28], we know that, for Euclidean domains, the mean critical stress (T_{crit}/N) is considerably smaller (about one half) than the mean bonding strength τ_{mean}.

Both in the case of Coulomb friction and of adhesion, performing numerical calculations on various contact domains, with different box dimensions Δ_S, shows that the larger the fractal dimension, the smaller the ratio $T_{\text{crit}}/T_{\text{nom}}$ (see Fig. 9(b), referring to the Coulomb case). This means that, in the case of rarefied contact domains within a fault, the partial-slip stage can develop more efficiently than in the case of dense Euclidean domains, and thus the transition to full-sliding is more ductile. This can be explained by the presence of large zones where contact does not occur, which represent a sort of *'slip-arresters'* preventing full-sliding (*gaps*). There is thus another correspondence between the classical instabilities associated to the fracture of brittle materials and the instabilities arising in faults sliding, as commonly detected, e.g., by acoustic emissions.

In the case of non-constant bonding strengths (e.g., strengths distributed according to Eq. (13)), we eventually found that, as the distributions tend to become more disordered, the ratio between T_{crit} and T_{nom} increases too.

6. Conclusions

A new numerical algorithm has been implemented in order to obtain the generalized fractal dimension of any multifractal distribution. It is based on an extension of the classical box-counting method, and does not require any

previous calculation of the correlation integral. This numerical tool was applied to the Italian catalogue of earthquakes, emphasizing how the released seismic energy obeys to multifractal scaling. It is worth noting the importance of the choice of the parameter (i.e., the seismic energy), in order to avoid the ambiguities found by other authors who considered the magnitude.

Moreover, it has been shown that the distribution of micro-forces between rough surfaces in contact is also multifractal. Finally, renormalization techniques have been applied to determine the tangential load capacity of self-affine faults, under the hypothesis of Coulomb's or adhesive contact law.

It is believed that further studies on the critical aspects of the sliding mechanics of natural faults should give deeper insight onto the origin of multifractal patterns in seismicity.

Acknowledgements

The present research was carried out with the financial support of the Ministry of University and Scientific Research (MURST), the National Science Foundation (CNR) and the EC-TMR Contract No. ERBFMRXCT 960062.

References

[1] Bak P, Tang C. Earthquakes as self-organized critical phenomena. J Geophys Res 1989;94:15635–7.
[2] Borodich FM. Renormalization schemes for earthquake prediction. Geophys J Int 1997;131:171–8.
[3] Borri-Brunetto M, Chiaia B, Ciavarella M. Incipient sliding of rough surfaces in contact: a multi-scale numerical analysis. Comput Meth Appl Mech Eng 2001;190:6053–73.
[4] Borri-Brunetto M, Carpinteri A, Chiaia B. Scaling phenomena due to fractal contact in concrete and rock fractures. Int J Fract 1999;95:221–38.
[5] Borri-Brunetto M, Chiaia B, Invernizzi S. Lacunar fractality of the contact domain in a closed rock fracture. In: Carpinteri A, Brebbia CA, editors. Damage and fracture mechanics: computer assessment and control. Southampton: Computational Mechanics Publications; 1998. p. 545–54.
[6] Burridge R, Knopoff L. Model and theoretical seismicity. Bull Seismol Soc Am 1967;57(3):341–71.
[7] Camassi R, Stucchi M. NT4.1 Un catalogo parametrico di terremoti di area italiana al di sopra della soglia del danno. Available from: http://emidius.itiin.mi.cnr.it/NT/hoine.htinl, Consiglio Nazionale delle Ricerche, Gruppo Nazionale per la Difesa dai Terremoti, Italy, 1996.
[8] Carpinteri A, Chiaia B. Power scaling laws and dimensional transitions in solids mechanics. Chaos, Solitons & Fractals 1996;7:1334–64.
[9] Eneva M. Effect of limited data sets in evaluating the scaling properties of spatially distributed data: an example from mining-induced seismic activity. Geophys J Int 1996;124:773–86.
[10] Feder J. Fractals. New York and London: Plenum Press; 1988.
[11] Godano C, Alonzo ML, Bottari A. Multifractal analysis of the spatial distribution of earthquakes in southern Italy. Geophys J Int 1996;125:901–11.
[12] Godano C, Caruso V. Multifractal analysis of earthquake catalogues. Geophys J Int 1995;121:385–92.
[13] Grassberger B, Procaccia I. Measuring the strangeness of strange attractors. Physica 1983;9(D):89–208.
[14] Gutenberg B, Richter CF. Earthquake magnitude intensity, energy and acceleration. Bull Seismol Soc Am 1942;32:162–91.
[15] Harlow DG, Phoenix SL. Probability distributions for the strength of fibrous materials under local load sharing. Two-level failure and edge effects. Adv Appl Probab 1982;14:68–94.
[16] Johnson KL. Adhesion and friction between a smooth elastic spherical asperity and a plane surface. Proc R Soc London A 1997;453:163–79.
[17] Kanamori H, Anderson DL. Theoretical basis of some empirical relations in seismology. Bull Seismol Soc Am 1975;65(5):1073–5.
[18] Kuge K, Lay T. Systematic non-double-couple components of earthquake mechanisms: the role of fault zone irregularity. J Geophys Res 1994;98(B8):15457–67.
[19] Main I. Is the reliable prediction of individual earthquakes a realistic scientific goal? Available from: http://helix. nature. com/debates/earthquake/equake_frameset.html, Nature Web Debates, moderator I. Main, 1999.
[20] Mosolov A. Singular fractal functions and mesoscopic effects in mechanics. Chaos, Solitons & Fractals 1994;4:2093–102.
[21] Olami Z, Feder JHS, Christensen K. Self-organized criticality in a continuous, non-conservative cellular automaton modeling earthquakes. Phys Rev Lett 1992;68(8):1244–7.
[22] Omori F. On the aftershocks of earthquakes. J Coll Sci Imp Univ Tokyo 1894;1:111–200.
[23] Ouillon G, Castaing C, Sornette D. Hierarchical geometry of faulting. J Geophys Res 1996;101(B3):5477–87.
[24] Reid HF. The mechanics of the earthquake. The California Earthquake of April 18, 1906, Report of the State Earthquake Investigation Commission, 2. Carneige Istitution of Washinton DC, 1910.
[25] Rice JR. Spatio-temporal complexity of slip on a fault. J Geophys Res 1993;98(B6):9885–907.

[26] Robertson MC, Sammis CG, Sahimi M, Martin AJ. Fractal analysis of three-dimensional spatial distributions of earthquakes with a percolation interpretation. J Geophys Res 1995;100(B1):609–20.
[27] Saleur H, Sammis C, Sornette D. Discrete scale invariance, complex fractal dimensions, and log-periodic fluctuations in seismicity. J Geophys Res 1996;101(B8):17661–77.
[28] Smalley RF, Turcotte DL, Solla SA. A renormalization group approach to the stick-slip behaviour of faults. J Geophys Res 1985;90:1894–900.
[29] Turcotte DL. Fractals and Chaos in Geology and Geophysics. Cambridge: Cambridge University Press; 1992.
[30] Wang JH, Lee CW. Multifractal measures of time series of earthquakes. J Phys Earth 1997;45:331–45.
[31] Wang W, Scholz CH. Scaling of constitutive parameters of friction for fractal surfaces. Int J Rock Mech Min Sci & Geomech Abstr 1993;7:1359–65.
[32] Yomogida K, Nakata T. Seimograms explained by the slip distribution of the 1995 Hyogo-Ken Nambu earthquake. J Phys Earth 1997;45:155–65.